



East Asian Summer Monsoon moisture sustains summer relative humidity in the southwestern Gobi Desert, China: evidence from $\delta^{18}\text{O}$ of tree rings

Qiang Li^{1,2} · Yu Liu^{1,2,3} · Takeshi Nakatsuka⁴ · Keyan Fang⁵ · Huiming Song^{1,2} · Ruoshi Liu³ · Changfeng Sun^{1,2} · Gang Li⁶ · Ke Wang⁶

Received: 8 April 2018 / Accepted: 19 October 2018 / Published online: 27 October 2018
© Springer-Verlag GmbH Germany, part of Springer Nature 2018

Abstract

The dominant climate-controlling system of the southwestern Gobi Desert and its surrounding areas in China at interannual to centennial time scale has not been determined. It is necessary to improve our understanding of the humidity variations in the past and forcing mechanisms in the southwestern Gobi Desert to enhance the accuracy of climate model predictions and cope with future desert advance/retreat crises resulting from climate change. We measured the annual stable oxygen isotope ratio ($\delta^{18}\text{O}$) in the cellulose of four *Picea crassifolia* trees growing on the fringe of the southwestern Gobi Desert from 1806 to 2011. Our tree-ring cellulose $\delta^{18}\text{O}$ values (34.49‰) were considerably higher than those reported in other regions of Asia, suggesting that the southwestern Gobi Desert has been extremely arid over the past two centuries. The chronology of tree-ring cellulose $\delta^{18}\text{O}$ is significantly ($p < 0.01$) negatively correlated with summer (June, July, and August) relative humidity (RH) records from 12 meteorological stations nearby our study region (Table 1). Based on the high correlation ($r = -0.740$, $p < 0.0001$, $n = 49$) between tree-ring cellulose $\delta^{18}\text{O}$ and instrumental summer RH from meteorological stations nearby our study region, we reconstructed summer RH variations during the past 206 years. Spatial correlation patterns between our reconstruction and several hydroclimate-related gridded data sets indicate that the reconstruction is representative of hydroclimate variations over a large area. Close agreement was observed between our reconstruction and several East Asian Summer Monsoon-related hydroclimate records. Our study indicates that the moisture from the east has introduced the RH to the southwestern Gobi Desert during the summer months over the past two centuries.

Keywords Tree rings · Stable oxygen isotope · Relative humidity · Gobi Desert · East Asian Summer Monsoon

1 Introduction

As the most dramatic climatic phenomenon on the Earth, the Asian Monsoon influences nearly two-thirds of human beings (An et al. 2015). During summer, the monsoon brings heavy rains to south and east Asia and adjacent

marginal seas. During winter, the airflow changes direction to cause a large amount of rainfall over Indonesia, north Australia, and the southern Pacific convergence zones (Clift and Plumb 2008). It is generally accepted that the East Asian Summer Monsoon (EASM, a branch of the Asian Monsoon system in summer), is the dominant

✉ Qiang Li
liqiang@ieecas.cn

✉ Yu Liu
liuyu@loess.llqg.ac.cn

¹ State Key Laboratory of Loess and Quaternary Geology, Institute of Earth Environment, Chinese Academy of Sciences, Xi'an 710061, China

² Interdisciplinary Research Center of Earth Science Frontier (IRCESF) and Joint Center for Global Change Studies (JCGCS), Beijing Normal University, Beijing 100875, China

³ School of Human Settlements and Civil Engineering, Xi'an Jiaotong University, Xi'an 710049, China

⁴ Research Institute of Humanity and Nature, 457-4 Motoyama, Kamigamo, Kita-ku, Kyoto 603-8047, Japan

⁵ Key Laboratory of Humid Subtropical Eco-geographical Process (Ministry of Education), College of Geographical Sciences, Fujian Normal University, Fuzhou 350007, China

⁶ Dongdashan Natural Reserve, Ganzhou District, Zhangye 734000, China

climate-controlling system over much of middle and eastern China. The modern boundary between the monsoonal and non-monsoonal areas is defined as the 200–400 mm isohyet of mean annual precipitation in China (dashed line in Fig. 1b) at an inter-annual time scale (An et al. 2012). The results of some studies support the above Modern Summer Monsoon Limit. For example, an annual precipitation reconstruction based on tree-ring widths in the Northern Mountains of the Hexi Corridor, which is in the northwest region of the Modern Summer Monsoon Limit, suggested that the local climate was dominated by westerlies (Chen et al. 2013). Additionally, stable oxygen isotopes of precipitation indicated that the westerly

circulation transfers water vapor to the central Hexi Corridor (Li et al. 2015a).

However, there have been disagreements regarding the dominant climate-controlling system in the northwest region at different time scales, especially in the southwestern Gobi Desert (Yu et al. 2006; Yang et al. 2011; Chen et al. 2013, 2016). During the middle Holocene, a strong EASM resulted in wetter climates in the Badain Jaran Desert of the southwestern Gobi Desert (Yang et al. 2010, 2011). In the middle Qilian Mountains of the Hexi Corridor, an analysis of tree-ring widths indicated that annual precipitation was controlled by the EASM in the past centuries (Yang et al. 2011). A study of the lake sediment record indicated that

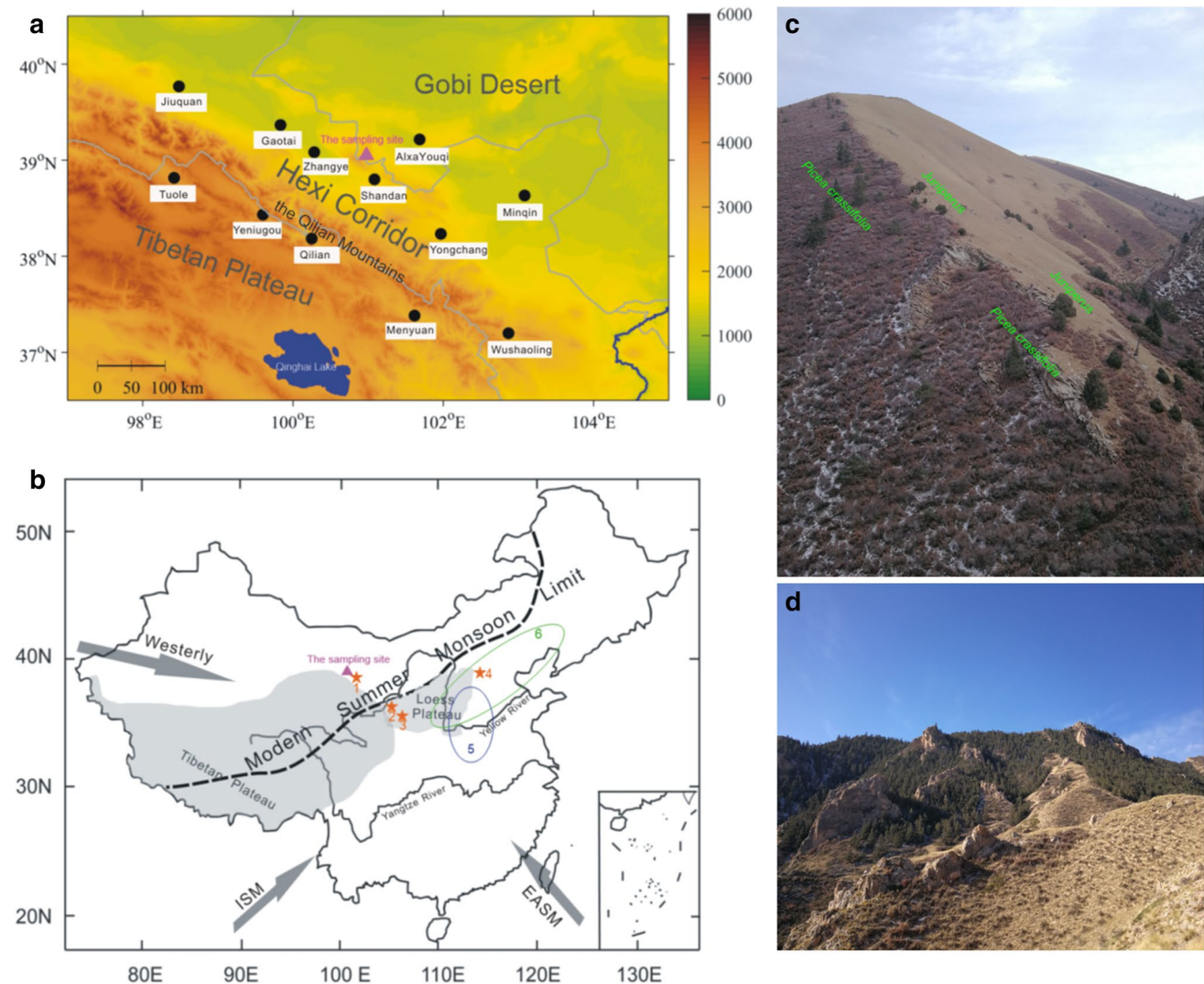


Fig. 1 Map **a** showing the sampling site (purple triangle) and all available meteorological stations (black solid circles); color bar shows altitudinal gradient (m; above sea level); map **b** showing locations of proxy records compared in this study: (1) JJA PDSI (38°45'N, 101°15'E, Cook et al. 2010), (2) Liancheng (Liu et al. 2013a), (3) Mt. Xinglong (Liu et al. 2013b), (4) Ningwu (Li et al.

2015b), (5) Regional JJA precipitation reconstruction in North China (Yi et al. 2012) and (6) Decadal precipitation reconstruction in North central China (Tan et al. 2011); ISM means Indian Summer Monsoon; **c** the upper limit and **d** lower limit of the forest in Longshou Mountain. (Photos were taken in October 2017)

the climate of the central Hexi Corridor was simultaneously regulated by westerlies and the EASM (Yu et al. 2006). Chen et al. (2016) noted the dominance of the EASM based on a temperature reconstruction from the tree rings of Zhangye (a city in the Hexi Corridor) during 1760–2006.

Understanding high-resolution humidity variability and relevant climate-controlling systems in marginal deserts is of great importance. Stabilized surface sand benefits from wetter conditions, because desert plants, such as shrubs, can rapidly grow and propagate, thereby reducing land desertification and the frequency of sandstorms. On the other hand, dry climates can trigger the degradation of ecosystems in marginal deserts, which can result in desert expansion and frequent sandstorm events. Tree rings, which provide accurate and absolute dating over a wide distribution, play an important role in high-resolution paleoclimate reconstruction around desert and arid regions (Dean et al. 1996; McCarroll and Loader 2004; Olson et al. 2017; Xu et al. 2018). With the advantages of good inter-series correlation, minimal influence of external disturbances, and close correlation to hydroclimatic variables, the stable oxygen isotope ratio ($\delta^{18}\text{O}$) of tree-ring cellulose can potentially reconstruct relative humidity (RH). Tree roots transfer soil water to the leaves, where transpiration induces the relative enrichment of ^{18}O . The extent of transpiration depends on the vapor pressure deficit and stomatal conductance, both of which are related to RH. Therefore, tree-ring cellulose $\delta^{18}\text{O}$ can be used as a proxy for RH, especially in the arid and semi-arid areas (White et al. 1985; Roden et al. 2000; McCarroll and Loader 2004; Qin et al. 2015; Wernicke et al. 2017a; Xu et al. 2018).

The aim of this study was to investigate the history and potential climate forcing system of summer (June, July, and August; JJA) RH in the southwestern Gobi Desert over the past two centuries by measuring the $\delta^{18}\text{O}$ chronologies of four Qinghai spruce (*Picea crassifolia*) trees growing on the northeastern slope of Longshou Mountain in the Northern Mountains of the Hexi Corridor, Northwest China.

2 Materials and methods

2.1 Sampling site and materials

The sampling site (39°03'N, 100°46'E, altitude 2900–3200 m above sea level) is located on the northeastern slope of Longshou Mountain (Fig. 1). Longshou Mountain is a part of the North Mountains. The North Mountains form a barrier that prevents the desert from moving southwestward, which is important for the Hexi Corridor. On the other side of the Hexi Corridor, the Qilian Mountains along the border of the Tibetan Plateau supply meltwater to the Hexi Corridor (Fig. 1). Benefiting from this topography, the Hexi Corridor

is one of the most important agricultural areas in Northwest China, and it has been serving as an important (one of the most important globally) trade route over the past ~2000 years (Liu and Shaffer 2007).

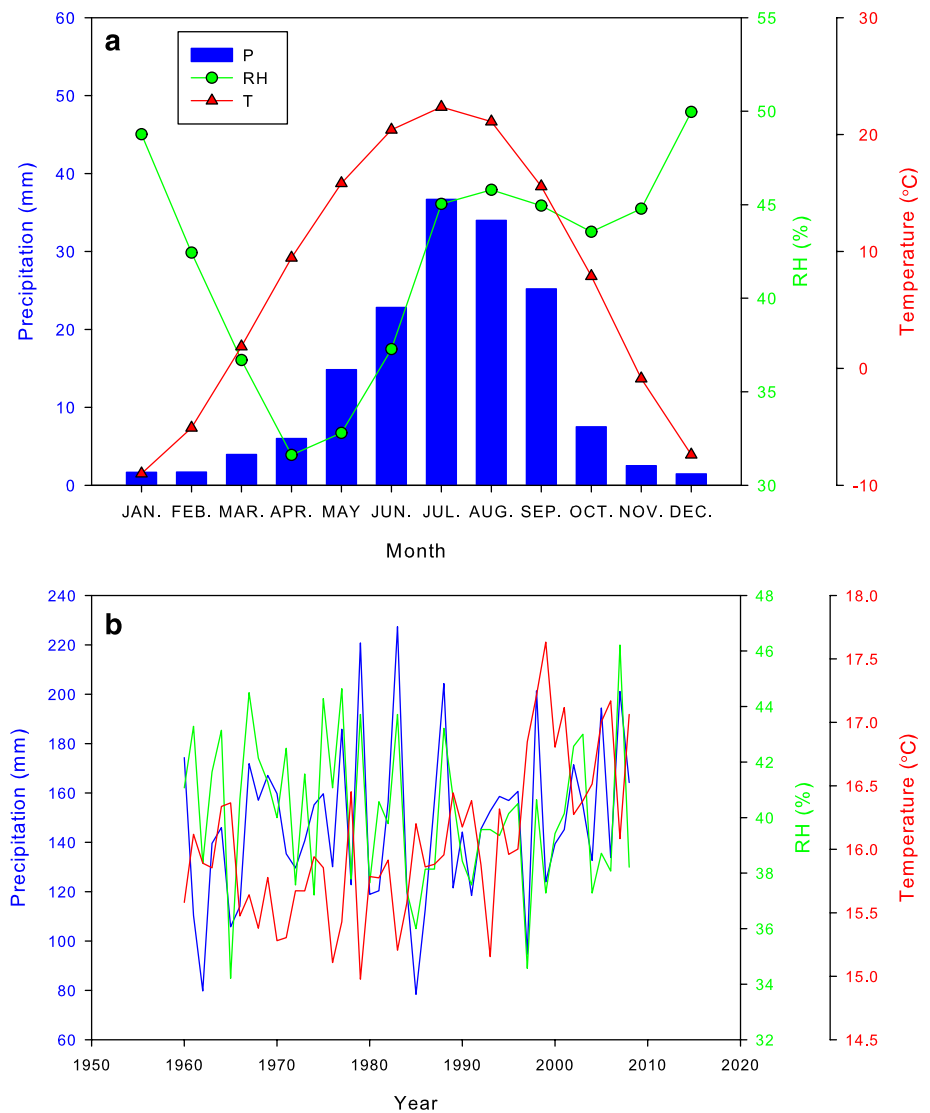
The northeastern slope of the Longshou Mountain faces the Badain Jaran Desert and the Tengger Desert, which are located along the southwest border of the largest desert in Asia (the Gobi Desert). Overall, 36 trees were sampled over an altitudinal gradient of 2900–3200 m. The vegetation at the sampling site is sparse, and species include Qinghai spruce, Juniper (*Sabina przewalskii* Kom.), and shrubs (*Salix cupularis*, *Aster divaricatus* Raf. and so on). *Picea crassifolia* is a unique species in China, which is distributed across the shady-slopes of mountains at an altitude of 1600–3800 m in the Qilian Mountains, the Qinghai Province, the Gansu Province, the Ningxia Hui Autonomous Region, and the Inner Mongolia Autonomous Region of Northwest China. The *Picea crassifolia* forest in the Qilian Mountains is characterized by lower soil bulk weight and higher soil water infiltration rate. The vertical distribution of soil water is mainly affected by precipitation (Dang et al. 2004). The dominant *Picea crassifolia* species were collected with two cores per tree in the upper reaches of the forest using a 12-mm-diameter tree ring borer at breast height. A total of 66 cores of *Picea crassifolia* were used for cross-dating, and the temperature during May–October was reconstructed based on the tree-ring width of those samples (Liu et al. 2016).

2.2 Local climate

The following climate records are based on average data of the Shandan and Alxa Youqi meteorological stations. During the instrumental observation (1960–2011), the mean annual precipitation (P) was 158 mm, 60% of which occurred in summer (JJA). The actual precipitation in the sampling site is significantly more than 158 mm/year because the altitude of the sampling site (2900–3200 m above sea level) is higher than that of the meteorological station (1600–1700 m above sea level). As shown in Fig. 1c, sparse *Juniperus* trees have been found in the upper limits of the forest at the sampling site. Mische et al. (2008) reported that the drought line for *Juniperus* forests in the Tibetan Plateau is approximately 200–250 mm/year. Therefore, the annual precipitation in the sampling site must be at least 200–250 mm.

The annual mean temperature (T) was 7.68 °C, with the hottest monthly mean temperature being recorded in July (22.36 °C) and the coldest monthly mean temperature being recorded in January (−9.01 °C). Two peaks in RH occurred, one in winter and the other in summer (Fig. 2). The former RH peak could be caused by a low saturation vapor pressure during the cold winter months. The latter peak of RH was probably caused by large amounts of rain in summer. From

Fig. 2 **a** Monthly mean P, RH, and T and **b** inter-annual P, RH, and T variations of average climate records from Shandan and Alxa Youqi meteorological stations during 1960–2008



the early stage to late stage of the growing season (April to October) (Liu et al. 2012a), the meteorological records show that the long-term RH trend was slightly downward ($-0.033\%/year$), whereas P and T exhibit upward trends of 0.467 mm/year and $0.025\text{ }^{\circ}\text{C/year}$, respectively.

2.3 Measurement of stable oxygen isotopes in tree rings

To find more climate signals, we selected four tree-ring samples to conduct the cellulose $\delta^{18}\text{O}$ analyses in the current study. The selected criteria are that samples should not have missing rings, false rings, and extremely narrow rings. The annual rings were carefully cut into thin sections with a razor blade under a binocular microscope. The boundary between earlywood and latewood was indistinct, which only permitted the separation of the entire annual ring. Within the wood components, α -cellulose is a very stable natural biopolymer,

which does not exchange stable carbon and oxygen isotopes after the original fixation of light elements (Leavitt 2010). The α -cellulose in the thin sections of the annual ring was extracted with a modified Jayme-Wise method (Loader et al. 1997). Briefly, the process includes using organic reagents, mixed solution of sodium chlorite, and 17.5% solution of sodium hydroxide to remove extractions (resin, ash and so on), lignin, and hemicellulose, respectively. The α -cellulose of the annual material was homogenized by using an ultrasonic cell disruptor. Approximately 0.13–0.17 mg of homogeneous α -cellulose was loaded into a silver capsule. The stable oxygen isotope ratio was determined with a pyrolysis-type elemental analyzer (ThermoFisher TC/EA) and an isotope ratio mass spectrometer (ThermoFisher Delta V Advantage) at the Research Institute of Humanity and Nature, Kyoto, Japan. The tree-ring stable oxygen isotope ratios were calculated by comparison with an isotope ratio that was predetermined using commercial cellulose standard

(27.7‰ VSMOW, Merck cellulose, Darmstadt, Germany). The Merck cellulose was inserted after every eight samples during the measurement process. The oxygen isotope ratios were expressed as $\delta^{18}\text{O}$, which represents the permil deviation relative to the Vienna Standard Mean Ocean Water (VSMOW). The analytical uncertainty of repeated measurements of the commercial cellulose was 0.2‰ (1σ).

2.4 Climatic data

All the observed P, RH, and T data from the 12 meteorological stations (Fig. 1; Table 1) were obtained from the China Meteorological Service Centre (<http://data.cma.cn/>). The duration of the data collected from the meteorological stations is 1960–2008 for RH, and 1960–2011 for P and T. The optimal climate parameter with the highest correlation coefficient with $\delta^{18}\text{O}$ was reconstructed in this study. The homogeneity of observed climate data was verified using the Mann–Kendall method (Liu et al. 2016).

Due to the uneven distribution of meteorological stations, we employed the following six global homogenized hydroclimate-related data sets (reanalysis gridded climate data) to assess the spatial representativeness of the reconstruction. (1) HadCRUH RH: It is a homogenized, quality controlled, near-global, 5° by 5° gridded monthly mean anomaly dataset on relative humidity for 1973–2003 from the Met Office Hadley Centre and Climatic Research Unit Global Surface Humidity dataset, (<http://www.cru.uea.ac.uk/data>), (Willett et al. 2008). (2) CRU TS3.2.1: precipitation (<http://www.cru.uea.ac.uk/data>). (3) CRU TS3.2.1: cloud fraction (<http://www.cru.uea.ac.uk/data>). (4) CRU self-calibrating Palmer Drought Severity Index (scPDSI, <http://www.cru.uea.ac.uk/data>) 3.2.1: PDSI is a popular drought index, which is calculated by combining the antecedent monthly precipitation,

temperature, moisture supply, and moisture demand into a water balance model. There is no unit for PDSI. Detailed information on PDSI is provided in Dai et al. (2004). The three aforementioned CRU datasets show month-by-month variation in climate parameters during 1901–2011. They are produced by the Climatic Research Unit (CRU) at the University of East Anglia, and were calculated on high-resolution ($0.5^\circ \times 0.5^\circ$) grids (Harris et al. 2014). (5) CSIC Standard Precipitation Evaporation Index (SPEI, <https://digital.csic.es/handle/10261/72264>): SPEI is designed to take into account both precipitation and potential evapotranspiration in determining droughts during 1901–2011, which captures the main impact of increased temperatures on water demand. It can be calculated on timescales ranging from 1 to 48 months. Detailed information on SPEI is provided in Beguería et al. (2014). The SPEI dataset is available from 1901 to 2011. (6) Standard Precipitation Index from Global Integrated Drought Monitoring and Prediction System and Global Land Data Assimilation System (SPI, <http://drought.eng.uci.edu/>) data sets. SPI is the number of standard deviations by which the observed cumulative precipitation deviates from the climatological average during 1949–2008. Detailed information on SPI is provided in Guttman (1999). High values of PDSI, SPEI, and SPI represent wetter conditions, while low values indicate drier conditions.

2.5 Statistical analyses

For the purpose of climate reconstruction, a linear regression model was constructed involving the primary cellulose $\delta^{18}\text{O}$ chronology and climatic data from the nearby meteorological stations (Fig. 1; Table 1). The Bootstrap and Jackknife methods were employed to verify the stability and reliability of our reconstruction. The assumption in the bootstrap is that

Table 1 Meteorological stations available in the surrounding areas

Meteorological stations	Location	Altitude (m a.s.l)	Periods (years)	Distance (km)
Hexi Corridor or Gobi Desert				
Zhangye (ZY)	38°56'N/100°26'E	1483	1951–2010	33
Shandan (SD)	38°48'N/101°05'E	1765	1953–2010	35
AlxaYouqi (AYQ)	39°13'N/101°41'E	1510	1959–2010	77
Jiuquan (JQ)	34°46'N/98°29'E	1477	1951–2010	212
Gaotai (GT)	39°22'N/99°50'E	1332	1953–2010	93
Yongchang (YC)	38°14'N/101°58'E	1976	1959–2010	138
Minqin (MQ)	38°38'N/103°05'E	1367	1953–2010	202
Tibetan Plateau				
Tuole (TL)	38°48'N/98°25'E	3367	1957–2010	209
Yeniugou (YNG)	38°25'N/99°35'E	3320	1960–2010	126
Qilian (QL)	38°11'N/100°15'E	2789	1957–2010	108
Menyuan (MY)	37°23'N/101°37'E	2851	1957–2010	199
Wushaoling (WSL)	37°12'N/102°52'E	3043	1952–2010	274

Distance refers to the distance from the sampling site

the available observations contain information necessary to construct an empirical probability distribution of any statistic of interest. The principle is that the original data are re-sampled several times to simulate sampling variability, providing an approximation of the unknown population (Efron 1979). A large number of iterative calculations were used in the Bootstrap method. The Jackknife method involves the calculation of the correlation of the time series after progressively removing 1 year throughout the time period. The basic idea of Jackknife lies in systematically recomputing the statistic estimate, leaving out one observation at a time from the sample set. From this new set of “observations” for the statistic, estimates for the bias and the variance of the statistic can be calculated (Quenouille 1949). The standard error of the estimate is a measure of the accuracy of predictions made with a regression line. When the standard error of the estimate in Jackknife and Bootstrap is close to that of the calibration period, it indicates that the regression line is better. In addition, the reduction of error (RE) and the coefficient of efficiency (CE) is common to check the reliability of our reconstruction in dendrochronology (Li et al. 2013). Our reconstruction was uploaded to a website of the KNMI Climate Explorer (<http://climexp.knmi.nl>) to evaluate

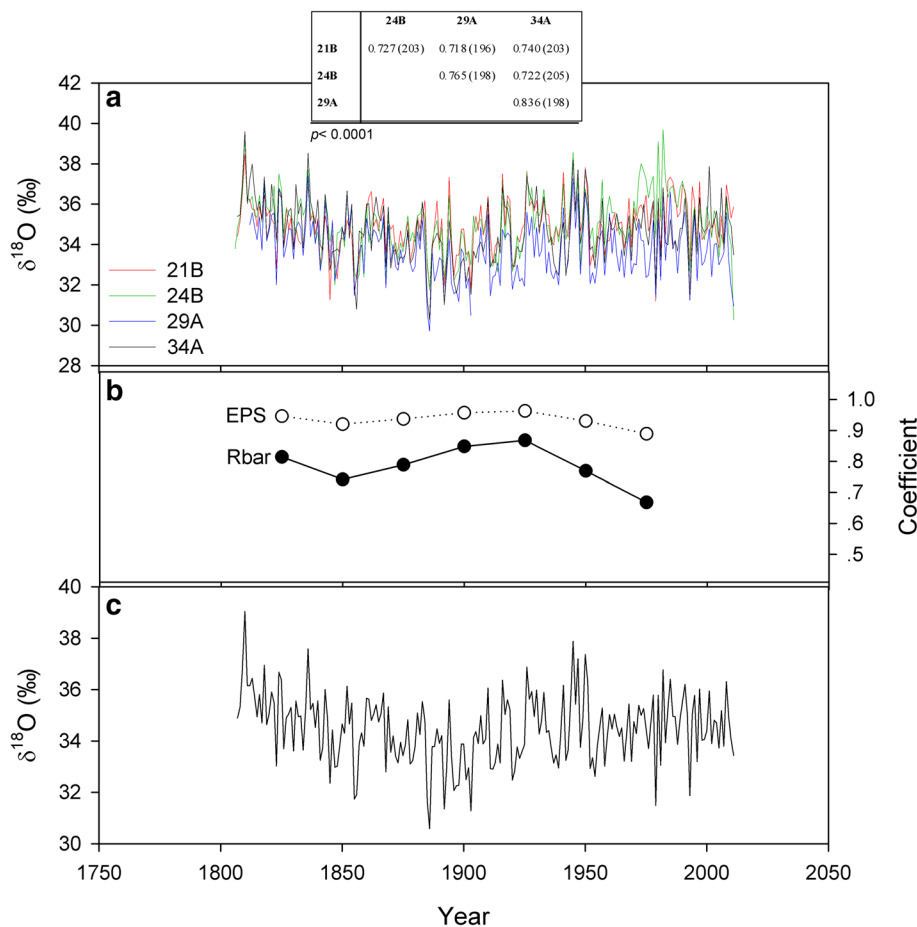
the spatial representativeness of our reconstruction by plotting spatial correlations between our reconstruction and six hydroclimate-related global gridded datasets (HadCRUH RH, CRU P, CRU cloud fraction, CRU PDSI, SPEI, and SPI). The first-order difference series was used to ensure that the high correlation of the original series was not caused by a long-term trend (Fig. 5d).

3 Results and discussion

3.1 Cellulose $\delta^{18}\text{O}$ chronology

We analyzed four cores reaching the pith (1807–2011 for Core 21B, 1806–2011 for Core 24B, 1812–2011 for Core 29A, and 1807–2011 for Core 34B). The cellulose $\delta^{18}\text{O}$ series of the four tree-ring cores corresponded to each another well (Fig. 3a). The correlations among the four cellulose $\delta^{18}\text{O}$ series ranged from 0.718 to 0.836. In Fig. 3b, the running (50-year window with a lag of 25 years) Expressed Population Signals (EPS) were higher than 0.85. Above this, the time series had an excellent ability to capture common regional signals (Wigley et al. 1984). In addition, the

Fig. 3 **a** Individual tree-ring cellulose $\delta^{18}\text{O}$ series and correlation coefficients with respect to each other; numbers inside of parenthesis are the overlapping years, **b** running EPS and Rbar statistics using 50-year windows with a 25-year lag, and **c** the mean tree-ring cellulose $\delta^{18}\text{O}$ chronology



running mean correlation coefficient (R_{bar} , 0.67–0.87) of the four cellulose $\delta^{18}\text{O}$ series is shown in Fig. 3b. The cellulose $\delta^{18}\text{O}$ values of 24B during the 1970s and 1980s were slightly higher than those of the other three cores (Fig. 3a). This difference may have been caused by changes in individual standing microenvironments. For example, soil layers could have become sparse, overly porous, or thin because of the activities of terrestrial life on the standing soil of 24B. These changes could have consequently increased soil water evaporation, which might have resulted in an enriched $\delta^{18}\text{O}$ in the soil water extracted by the tree roots. The high cellulose $\delta^{18}\text{O}$ values of 24B during the 1970s and 1980s are likely the reason for the decrease in EPS and R_{bar} values for the last point in Fig. 3b. These issues create some bias regarding the overall chronology. Therefore, we combined 21B, 29A, and 34B to constitute the mean cellulose $\delta^{18}\text{O}$ chronology to avoid any deviation induced by 24B (Fig. 3c). The EPS value can also be used to evaluate the minimum required number of trees and capture a representative isotope signal for a site (McCarroll and Loader 2004). The EPS value of the three cellulose $\delta^{18}\text{O}$ series (21B, 29A, and 34B) is 0.90, which is higher than the standard threshold value of 0.85. This result suggests that the mean of the three cellulose $\delta^{18}\text{O}$ chronologies in this study effectively captures the common signal of the tree-ring $\delta^{18}\text{O}$ variations in the sampling site. In addition, using individual measurements of tree-ring cellulose $\delta^{18}\text{O}$, it is not difficult to identify abnormal segments in isotopic measurements, such as that for 24B in this study, whereas the pooling of more trees prior to measurement may lead to errors in the cellulose $\delta^{18}\text{O}$ series.

3.2 The relatively higher cellulose $\delta^{18}\text{O}$ value over Asia

The cellulose $\delta^{18}\text{O}$ values of the mean chronology range from 30.59 to 39.04‰, with the average being $34.49 \pm 1.33\text{‰}$. The mean value is the relatively higher tree-ring cellulose $\delta^{18}\text{O}$ value in published studies across Asia (Ramesh et al. 1985; Treydte et al. 2006; Tsuji et al. 2006; Liu et al. 2008, 2012b; Nakatsuka et al. 2008; Sano et al. 2010; Li et al. 2011a, b, 2015a, b; Xu et al. 2011, 2015a, b; Wang et al. 2013; Qin et al. 2015; Wernicke et al. 2017a), including the cellulose $\delta^{18}\text{O}$ values in the arid northeastern Qaidam on the Tibetan Plateau (33.46‰, 33.31‰, and 32.20‰; Xu et al. 2011; Wang et al. 2013; Qin et al. 2015) and the southeastern Tibetan Plateau region (25‰; Shi et al. 2012). Cellulose $\delta^{18}\text{O}$ is primarily determined by precipitation (positive correlation) and RH (negative correlation; Li et al. 2011a). The higher cellulose $\delta^{18}\text{O}$ value in this study may be the result of inland precipitation enriched with $\delta^{18}\text{O}$, as opposed to precipitation in coastal areas due to Raleigh fractionation (Vuille et al. 2005). However, the cellulose $\delta^{18}\text{O}$ values in northern Pakistan (28.6–31.1‰;

Treydte et al. 2006) and the western Tianshan Mountains ($31.7 \pm 0.19\text{‰}$; Xu et al. 2015a, b) are lower than those observed in this study. Both northern Pakistan and the western Tianshan Mountains are farther from the ocean. This finding implies that the other influential factor, RH, may play a more important role in accounting for these high cellulose $\delta^{18}\text{O}$ values. The sampling site is located on the southwestern border of the Gobi Desert, which is drier than the study sites in the literature, which included northeastern Qaidam, the Altay Mountains, and northern Pakistan. Note that possible offsets exist due to different tree species. However, all of the cellulose $\delta^{18}\text{O}$ studies compared above investigated shallow-root conifers with similar physiological parameters, such as an ^{18}O enrichment level of 27‰ in leaf water because of transpiration and an exchange ratio of 36–42% of oxygen atoms between the sugars and xylem (source) water in the trunk (Roden et al. 2000). In addition, the instrumental observations suggested that the study area is an extremely dry region (Ma et al. 2011). Thus, it is reasonable to assume that an extremely low RH resulted in the high cellulose $\delta^{18}\text{O}$ values observed in this study. It should be noted that the fractionation process of *Picea crassifolia* $\delta^{18}\text{O}$ is not understood in detail at the current stage. There is still some uncertainty in the comparison above. More ecological studies of *Picea crassifolia* are necessary, such as that of the fractionation process and the role of precipitation $\delta^{18}\text{O}$ (Wernicke et al. 2017b).

3.3 Climate responses and spatial representativeness

There are 12 metrological stations in the surrounding area at a distance of 33–274 km from the sampling site (Fig. 1; Table 1). Seven of the stations are located on the Hexi Corridor (or the Gobi Desert) side of the border, while the others are located on the Tibetan Plateau side (Fig. 1). Although the climatic conditions and altitudes of the metrological stations differ (Table 1), the summer P and RH data from all of the metrological stations were negatively correlated with the cellulose $\delta^{18}\text{O}$ values based on instrumental observation during 1960–2008 (Fig. 4). This finding coincides with the physiological control of tree-ring cellulose $\delta^{18}\text{O}$ (Roden et al. 2000). Specifically, the summer RH at all stations exhibited significantly ($p < 0.01$) negative correlations with cellulose $\delta^{18}\text{O}$, regardless of the distance from the sampling site (Fig. 4). For example, the correlation coefficient of RH in JJA was -0.642 ($p < 0.001$, $n = 57$) at the Wushaoling meteorological station, a distant (274 km away) and high-altitude (3043 m above sea level) meteorological station in the border of the Tibetan Plateau. The results demonstrated that cellulose $\delta^{18}\text{O}$ was spatially representative of RH across the large study area. Correlation coefficients between the cellulose

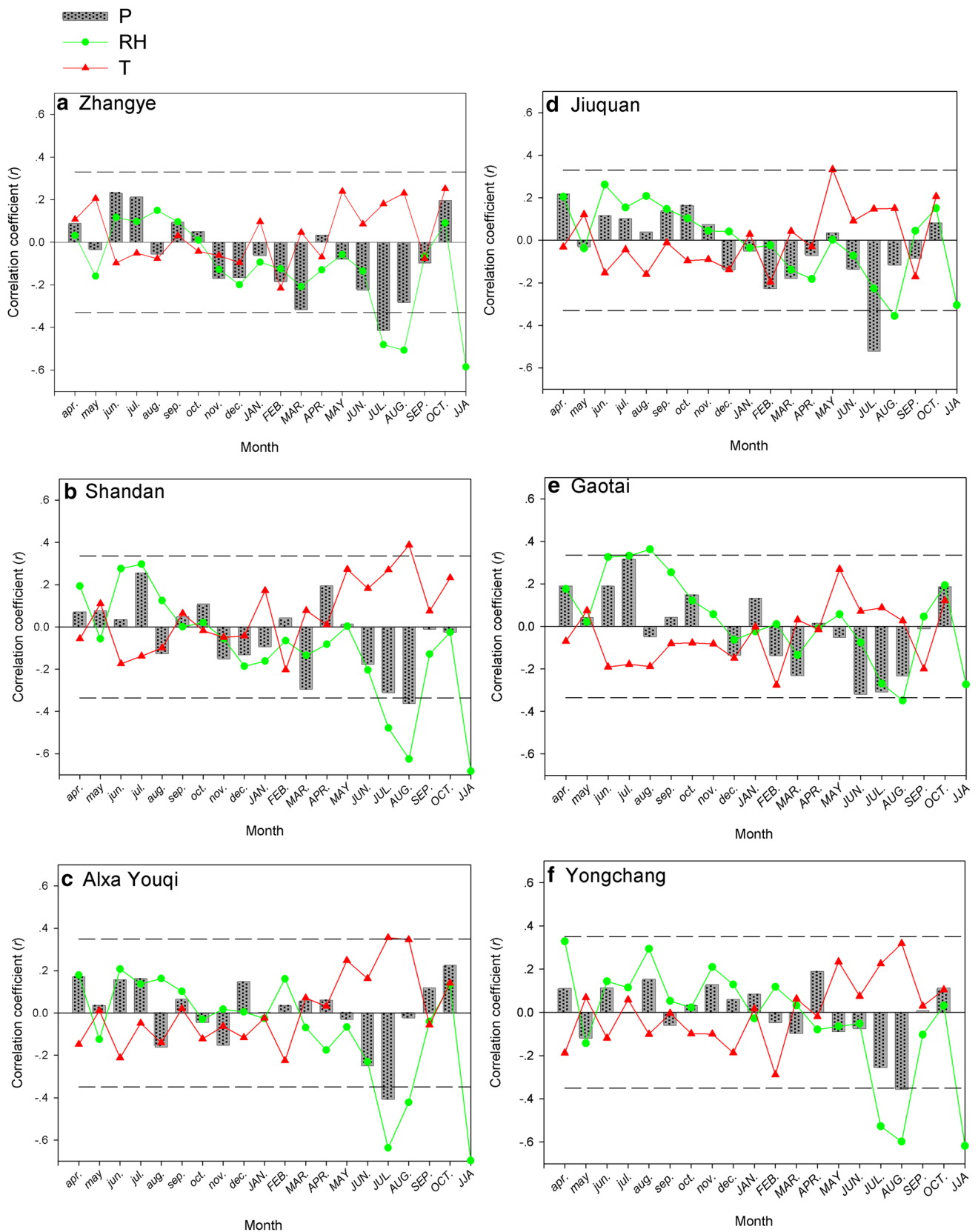


Fig. 4 Monthly correlation coefficients between the mean $\delta^{18}\text{O}$ chronology and P, RH, and T of the surrounding 12 meteorological stations. The month with lowercase/uppercase letters indicates

the month of the previous/current year; JJA means June, July, and August; dashed line indicates 99% confidence level

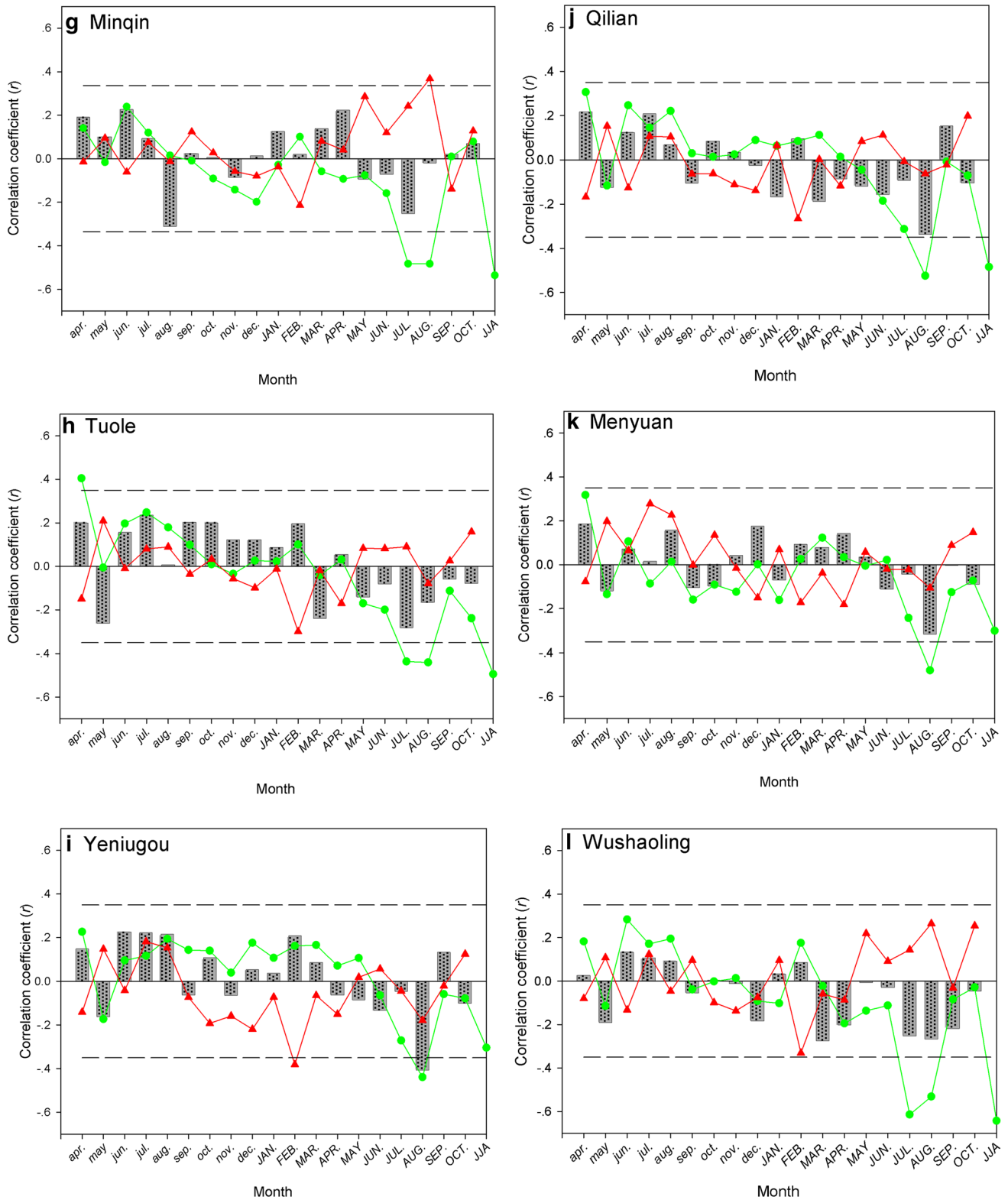


Fig. 4 (continued)

$\delta^{18}\text{O}$ and JJA RH of every meteorological station are shown in Fig. 4a. The JJA RH records from meteorological stations on the Tibetan Plateau side (Tuole, Yeniugou, Qilian, and Menyuan) and on the northwest side of the sample site (Jiuquan and Gaotai) have lower correlations with the cellulose $\delta^{18}\text{O}$. The JJA RH from other climate stations, including Wushaoling, Minqin, Yongchang, Shandan, and Alxa Youqi, have higher correlations with the cellulose $\delta^{18}\text{O}$. This may imply that moisture from the southeast of the sampling site is more important for the cellulose $\delta^{18}\text{O}$. Additionally, during the growing season, the shallow root system of *Picea crassifolia* cannot extract deep underground water that is mixed with winter water (Li et al. 2011a).

3.4 Absence of age-related trends in cellulose $\delta^{18}\text{O}$

In contrast to the tree-ring cellulose $\delta^{13}\text{C}$ that exhibits an age-related downward trend (juvenile effect), tree-ring cellulose $\delta^{18}\text{O}$ does not show a clear age-related trend (Leavitt 2010). In northern Pakistan, the tree-ring cellulose $\delta^{18}\text{O}$ values of a young juniper exhibited an obvious juvenile effect (Treydte et al. 2006). A short-term juvenile effect was observed in the cellulose $\delta^{18}\text{O}$ values of UK oak (Duffy et al. 2017). The cellulose $\delta^{18}\text{O}$ values of young oak trees from southwestern France exhibited a 2‰ upward trend in the first 30 years of growth (Labuhn et al. 2014). In northern China, one tree-ring cellulose $\delta^{18}\text{O}$ series of larch exhibited a juvenile effect, whereas the other series did not (Li et al. 2011b). The cellulose $\delta^{18}\text{O}$ values of Scots pine in northwestern Norway displayed no statistically significant juvenile effect (Young et al. 2011). In this study, a long-term downward trend (-0.03% /year) was observed in the first ~90 years (1807–1900s, or the nineteenth century) for all four cellulose $\delta^{18}\text{O}$ series (Fig. 3a). The downward trend for cellulose $\delta^{18}\text{O}$ could either be age-related or be the effect of climate signals. It is necessary to distinguish these for further climate reconstruction.

If we hypothesize that the downward trend in cellulose $\delta^{18}\text{O}$ was caused by actual climate variations, a long wetting trend (increasing RH) must have existed in the surrounding area during the nineteenth century because the cellulose $\delta^{18}\text{O}$ was significantly negatively correlated with the regional RH (Fig. 4). The hydroclimate reconstructions in the surrounding area reflected a common wetting trend during the nineteenth century. For example, from 1807 to 1900, the annual precipitation in Liancheng, western China, exhibited a 0.174 mm/year increase (Liu et al. 2013a). Additionally, the nearest grid point of the summer Palmer Drought Severity Index reconstruction (MADA 284) exhibited an upward trend of 0.002/year (Cook et al. 2010). Precipitation anomalies in north-central China [37°30'N, 103°00'E] exhibited a 0.023 mm/decade upward trend (Tan et al. 2011).

In the neighboring area of Jiuquan, annual precipitation has declined since the 1890s, following an upward trend from the 1720s to 1890s (Yang et al. 2011). All of the above comparisons suggest that the downward trend in cellulose $\delta^{18}\text{O}$ values was not caused by the juvenile effect. In addition, the length of the juvenile effect is generally approximately 30 years as reported by other studies (McCarroll and Loader 2004; Leavitt 2010). However, the downward trend of $\delta^{18}\text{O}$ in the beginning of our chronology is approximately 90 years. This is the other evidence suggesting that our tree-ring $\delta^{18}\text{O}$ chronology is not influenced by the juvenile effect. Thus, we use the entire length of the cellulose $\delta^{18}\text{O}$ series for climatic reconstruction.

3.5 Summer RH reconstruction

Although Zhangye is the nearest meteorological station, the cellulose $\delta^{18}\text{O}$ chronology only explained 32% ($r = -0.568$, $p < 0.0001$, $n = 60$) variance in the observed JJA RH in Zhangye. The North Mountains may obstruct the conveyance of moisture from Zhangye to the sampling site (Fig. 1), resulting in the Zhangye microclimate not reflecting the climatic signal of the sampling site. In fact, large amounts of glacier meltwater from the Qilian Mountains moisten Zhangye in the Hexi Corridor (Liu and Shaffer 2007). The mean annual RH of Zhangye (52%) was higher than that of Shandan (47%) and Alxa Youqi (37%) during the common period of 1959–2010.

The meteorological stations of Shandan and Alxa Youqi are located in the northeastern part of North Mountains, while the sampling site faces the Gobi Desert (Fig. 1). Therefore, we used the climatic data from Shandan, Alxa Youqi, and the average of Shandan and Alxa Youqi (SA) for correlation analysis. The most significant correlation coefficient was detected between cellulose $\delta^{18}\text{O}$ and the combined JJA RH from SA ($r = -0.740$, $p < 0.0001$, $n = 49$; Fig. 5a). The Pearson's correlation coefficients of P, T, and RH for SA are shown in Fig. 5a. The first-order autocorrelation coefficient of our tree-ring $\delta^{18}\text{O}$ chronology is 0.275, which indicates that the climate of the previous year has influenced the tree-ring $\delta^{18}\text{O}$ of the current year. However, Fig. 5a shows that the effect of climate record of the previous year is not significant ($p > 0.05$), which is reasonable. Tree-ring $\delta^{18}\text{O}$ is a ratio between ^{18}O and ^{16}O in cellulose. It is not related to tree growth. Based on tree physiology, tree-ring $\delta^{18}\text{O}$ is mainly determined by RH and $\delta^{18}\text{O}$ of soil water (Roden et al. 2000). In the beginning of growth period (spring), soil water may be mixed with melting snow (previous year's precipitation) and precipitation from the current spring. Due to the limited contribution of melting snow, the correlation between the tree-ring $\delta^{18}\text{O}$ and the climate records of the previous year is not significant. The purpose of this study was to reconstruct climate variations. Therefore, we selected

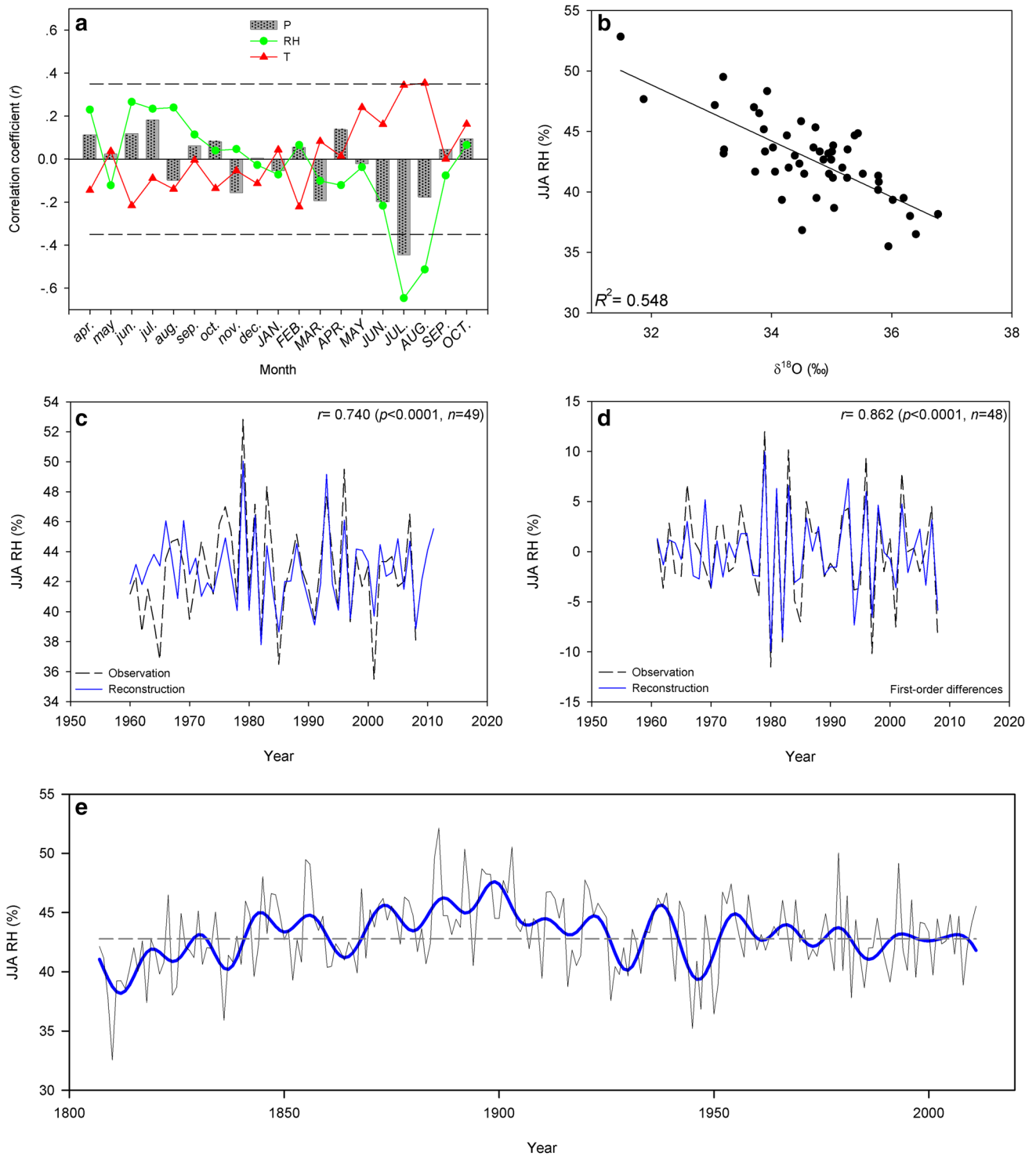


Fig. 5 **a** Monthly correlation coefficients between the tree-ring cellulose $\delta^{18}\text{O}$ chronology and instrumental P, RH, and T in the average data from Shandan and Alxa Youqi meteorological stations, **b** scatter diagram between instrumental summer RH and the tree-ring cellulose

$\delta^{18}\text{O}$, **c** comparisons between instrumental and reconstructed summer RH and **d** their first-order difference series, **e** reconstructed summer RH variation. The solid line is a 10-year low-pass filter

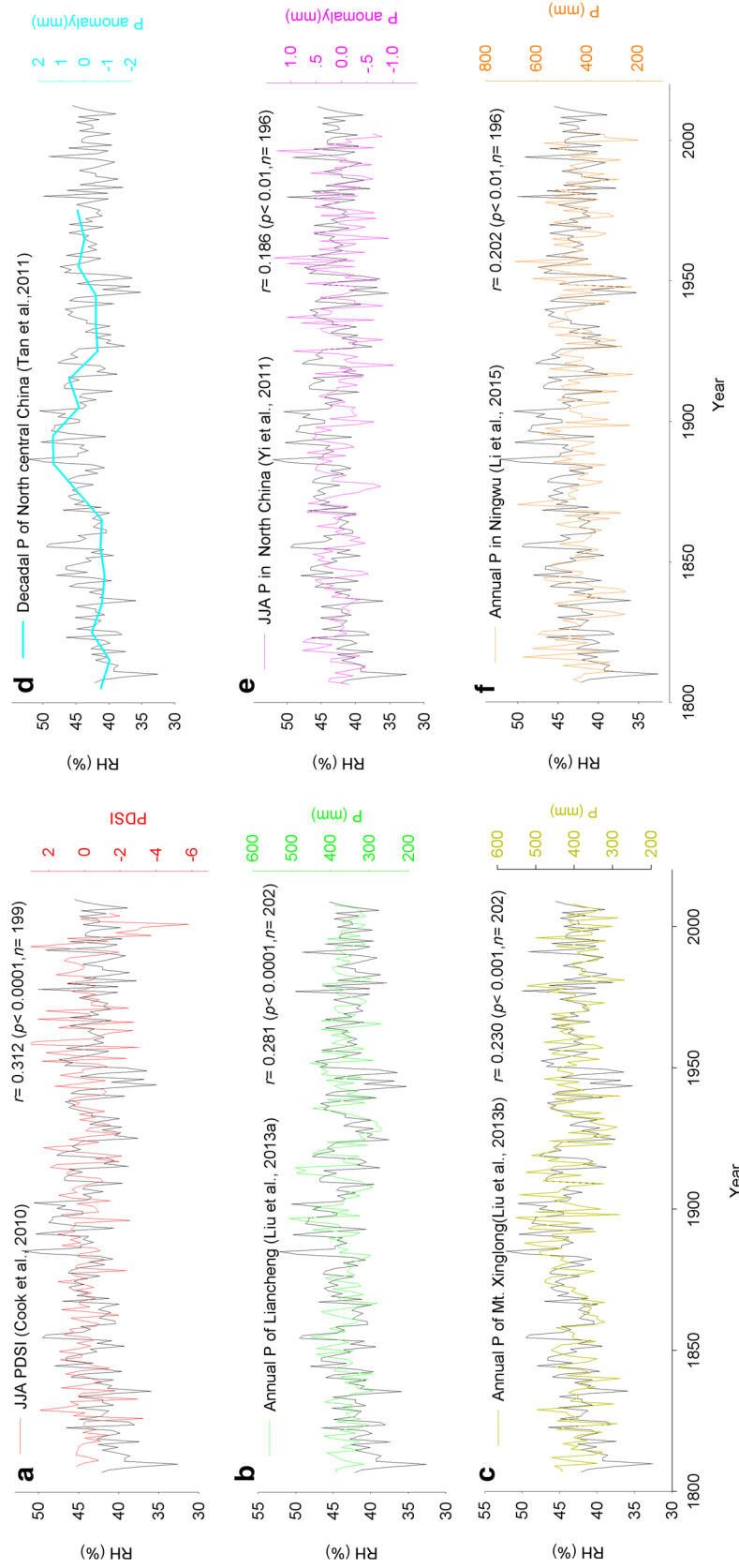


Fig. 6 Comparison between the reconstructed summer RH and **a** nearest JJA PDSI reconstruction, **b** annual P of Liancheng, **c** annual P of Mt. Xinglong, **d** decadal P of North central China, **e** summer P of North China, and **f** annual P of Ningwu

Table 2 Verification statistics of Jackknife and Bootstrap for the summer RH reconstruction

Statistical items	Calibration period (1960–2008)	Verification period (1960–2008)	
		Jackknife mean (range)	Bootstrap (50 iterations) mean (range)
r	0.74	0.72 (0.67–0.76)	0.72 (0.39–0.85)
R^2	0.54	0.52 (0.45–0.58)	0.52 (0.15–0.73)
R^2_{adj}	0.53	0.51 (0.44–0.57)	0.51 (0.13–0.72)
Standard error of estimate	88.00	88.00 (79.76–88.96)	87.48 (60.55–107.42)
F	56.93	50.02 (38.20–64.33)	52.26 (8.32–124.20)
p	0.0001	0.0001 (0.0001–0.0001)	0.0001 (0.0001–0.006)
Durbin–Watson	2.39	2.39 (2.18–2.54)	2.36 (2.11–2.54)
RE/CE	0.55		

the climate parameter with the highest correlation (June to August RH of current year) to carry out further analyses.

A linear regression function was employed to reconstruct the summer RH variations based on the tree-ring cellulose $\delta^{18}\text{O}$. The reconstruction explained 54.8% (53.8% after adjusting for the loss of degrees of freedom) of the variance in the observations (Fig. 5b). The reconstructed and observed summer RH exhibit significant consistency in both their original series (Fig. 5c) and first-order difference series (Fig. 5d).

In this study, 50 iterations were carried out in Bootstrap and Jackknife methods to check the stability and reliability of our reconstruction (Table 2). During the entire period, the reduction of error (RE) is the same as the coefficient of efficiency (CE) because the calibration and verification period is the same (Cook et al. 1994). The RE and CE were 0.55 in this study (Table 2). All statistic items in Table 2 indicate that the regression model is fairly stable and reliable.

As shown in Fig. 5e and the discussion in Sect. 3.4, from the beginning of the reconstruction to the 1890s, the reconstruction exhibited a wetting trend at the centennial scale (0.68%/decade), which is significantly correlated with the other hydroclimate series in the adjacent area. The spatial correlation between the reconstruction and the six gridded hydroclimate-related data sets is shown in Fig. 7, which illustrates that the JJA RH reconstruction effectively represents long-term hydroclimate variations in the entire southwestern Gobi Desert.

3.6 Effect of moisture from the east

Our reconstructed summer RH exhibits significant correlations with EASM-related hydroclimate reconstructions over north and north-central China. For example, the correlation coefficients between our summer RH reconstruction and the annual precipitation in Liancheng (Liu et al. 2013a) and Mt. Xinglong (Liu et al. 2013b) in north-central China, two regions influenced by the EASM, are 0.281 ($p < 0.0001$, $n = 202$) and 0.230 ($p < 0.001$, $n = 202$), respectively (Fig. 6c,

d). The JJA precipitation in monsoonal North China was reconstructed based on historical documents and tree-ring widths (Yi et al. 2012), which were significantly correlated with our summer RH reconstruction ($r = 0.186$, $p < 0.01$, $n = 196$; Fig. 6g). The annual EASM precipitation reconstruction in Ningwu, Shanxi Province, exhibits variations similar to those in our summer RH reconstruction ($r = 0.202$, $p < 0.01$, $n = 196$; Fig. 6h). In addition, a drying trend appears in the last century in our RH reconstruction. This trend may be related to the observed decline in the EASM since the end of the nineteenth century (Guo et al. 2004).

Conversely, our summer RH reconstruction does not display any characteristics of westerly circulation. An obvious drying trend was detected with regard to humidity in central Asia (Chen et al. 2010). In addition, the January to August SPEI reconstruction, which is based on the tree-ring $\delta^{18}\text{O}$ values from the western Tianshan Mountains, indicated that a strong westerly circulation has occurred since the late nineteenth century (Xu et al. 2015a, b). To the contrary, a trend from wet to dry began in the 1890s according to our RH reconstruction (Fig. 5). The annual precipitation reconstruction based on the tree-ring widths at the adjacent sampling sites (39°03'N, 100°43'E' and 38°56'N, 100°57'E; Chen et al. 2013) may have responded to the westerly circulation because it contains winter climate signals. In general, the westerly circulation is stronger in winter than in summer, whereas our reconstruction emphasized summer RH variations. Additionally, on the Hexi Corridor side of the border (Zhangye), annual precipitation was the main limiting factor of tree-ring widths, as noted by Chen et al. (2013). However, on the Gobi Desert side of the border (Shandan and Alxa Youqi), summer RH determined the tree-ring $\delta^{18}\text{O}$ ratio, as observed in the current study. Although the Hexi Corridor and the Gobi Desert are close, the North Mountains obstruct moisture convection between them.

Although the study area was considered uninfluenced by the Asian monsoons based on traditional understanding, considering the consistent variability in EASM-related reconstructions, the current study implies that the summer RH in the southwestern Gobi Desert is maintained by moisture

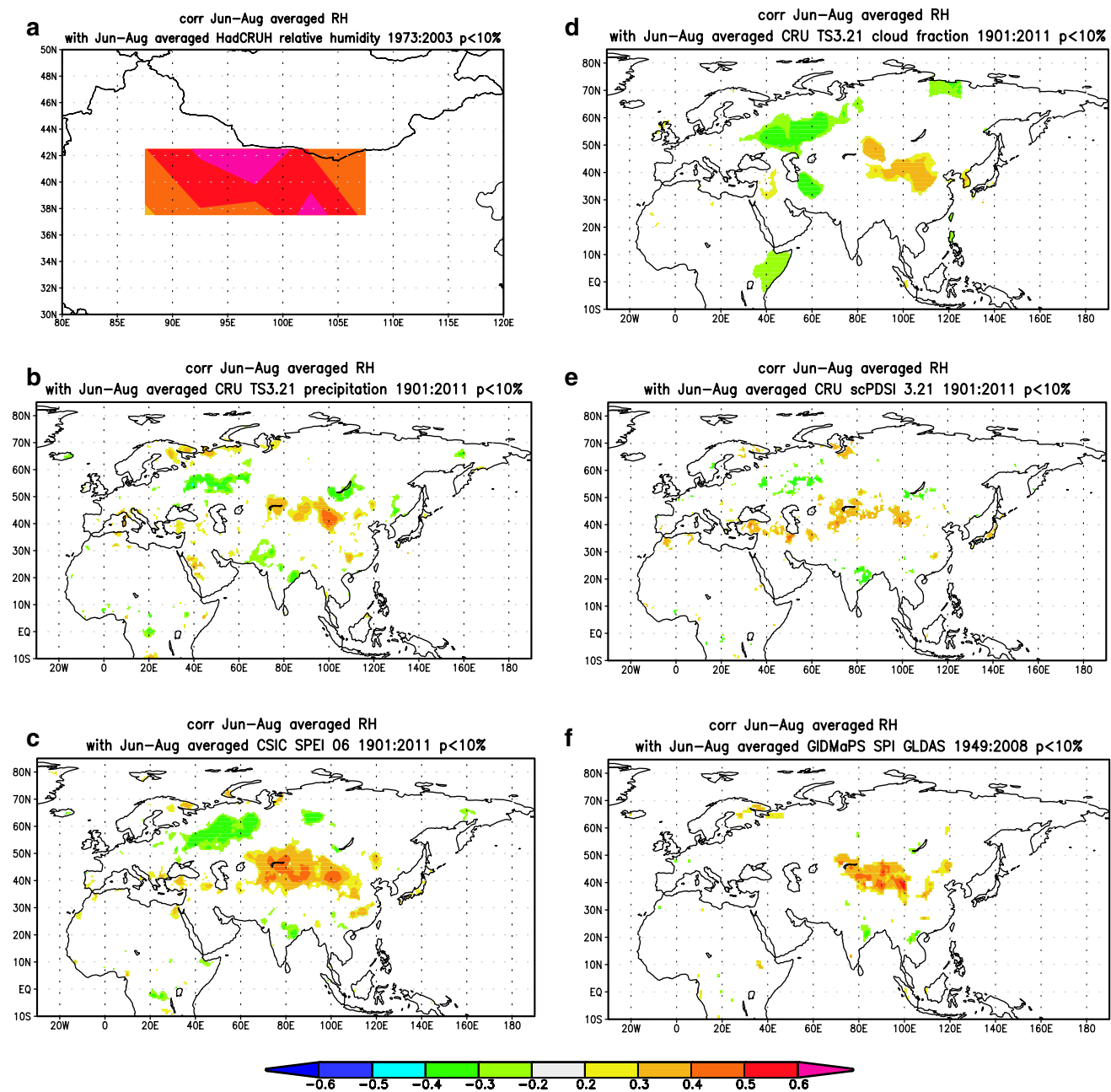


Fig. 7 Spatial correlation patterns between our reconstruction and a gridded summer HadCRUH relative humidity, **b** CRU TS3.2.1 precipitation, **c** CSIC Standard Precipitation Evaporation Index, **d** CRU TS3.2.1 cloud fraction, **e** CRU self-calibrating Palmer Drought Severity Index 3.2.1, and **f** Standard Precipitation Index from Global Inter-

grated Drought Monitoring and Prediction System and Global Land Data Assimilation System (GIDMaPS SPI GLDAS) datasets. The period in the correlation pattern depends on that of the gridded datasets

from the east. A teleconnection between precipitation in the EASM region and the East European Plain in summer has been confirmed by meteorologists, which is caused by the extension of stationary Rossby waves in the mid-latitudes in the upper troposphere in summer (Su and Lu 2014). In the spatial map (Fig. 7b–d), the teleconnection between our

reconstruction and moisture-related index of the East European Plain confirm that our sampling site belongs to the EASM region. Note that we emphasized the significance of the season (summer) in this study because the EASM is more prevalent in summer. Therefore, the moisture from the east can be conveyed to the southwestern Gobi Desert

by the EASM in summer. From late autumn to early spring, the predominant wind direction is from northwest because of the Siberian High (Gong and Ho 2002). In summer, with the weakening of the Siberian High, the study area is not affected by it. The EASM moisture could reach the study area, due to which the precipitation as per the climate station record was the highest in summer (Fig. 2a). However, more high-resolution hydroclimate studies are required to fully understand the climate change processes in the border area of the Gobi Desert.

4 Conclusions

We developed a 206-year tree ring cellulose $\delta^{18}\text{O}$ chronology based on trees growing on the northeast slope of Longshou Mountain in southwestern Gobi Desert. The tree-ring cellulose $\delta^{18}\text{O}$ chronology is significantly negatively correlated with the summer RH records from the surrounding 12 meteorological stations. Based on the highest correlation with meteorological records along the southwestern border of the Gobi Desert, we reconstructed summer (June, July, and August) RH variations over the past 206 years. The reconstruction explains 53.8% (after adjusting for the loss of degrees of freedom) of the variance in the instrumental record. The reconstruction indicated that the 1890s was the wettest decade, and the driest periods were the 1810s and the 1940s in the southwestern Gobi Desert during the past two centuries. The reconstructed summer RH exhibits synchronous variability and a significant ($p < 0.01$) correlation with several EASM-related hydroclimate series from North and Central China, implying the EASM has influenced climate change in southwestern Gobi Desert, at least during the summer months, over the past two centuries.

Acknowledgements We thank the anonymous reviewers for their valuable comments and suggestions. This study was financially supported by National Natural Science Foundation of China (nos. 41873021 and 41630531), CAS Key Research Program of Frontier Sciences (QYZDJ-SSW-DQC021, XDPB05, and GJHZ1777); Youth Innovation Promotion Association (no. 2017451) of CAS; West Light Foundation of CAS, Young Star of Science and Technology, Shaanxi Province; and Cultivating Foundation of SKLLQG. This work is a contribution of The Belt and Road Center of Environmental Studies, the Institute of Earth and Environment, Chinese Academy of Sciences.

References

- An Z, Colman SM, Zhou W, Li X, Brown ET, Jull AJT, Cai Y, Huang Y, Lu X, Chang H (2012) Interplay between the Westerlies and Asian monsoon recorded in Lake Qinghai sediments since 32 ka. *Sci Rep* 2:619
- An Z, Wu G, Li J, Sun Y, Liu Y (2015) Global monsoon dynamics and climate change. *J Earth Environ* 6:341–381
- Beguéría S, Vicente-Serrano SM, Reig F (2014) Standardized precipitation evapotranspiration index (SPEI) revisited: parameter fitting, evapotranspiration models, tools, datasets and drought monitoring. *Int J Climatol* 34(10):3001–3023
- Chen FH, Chen JH, Holmes J, Boomer I, Austin P, Gates JB, Wang NL, Brooks SJ, Zhang JW (2010) Moisture changes over the last millennium in arid central Asia: a review, synthesis and comparison with monsoon region. *Quat Sci Rev* 29:1055–1068
- Chen F, Yuan Y, Wei W, Zhang R, Yu S, Shang H et al (2013) Tree-ring-based annual precipitation reconstruction for the Hexi corridor, NW China: consequences for climate history on and beyond the mid-latitude Asian continent. *Boreas* 42(4):1008–1021
- Chen F, Yuan Y, Zhang T, Linderholm HW (2016) Annual precipitation variation for the southern edge of the Gobi Desert (China) inferred from tree rings: linkages to climatic warming of twentieth century. *Nat Hazards* 81:939–955
- Clift P, Plumb RA (2008) *The Asian monsoon*. Cambridge University Press, Cambridge
- Cook ER, Briffa KR, Jones PD (1994) Spatial regression methods in dendroclimatology: a review and comparison of two techniques. *Int J Climatol* 14(4):379–402
- Cook ER, Anchukaitis KJ, Buckley BM, D'Arrigo RD, Jacoby GC, Wright WE (2010) Asian monsoon failure and megadrought during the last millennium. *Science* 328:486
- Dai A, Trenberth KE, Qian T (2004) A global data set of Palmer drought severity index for 1870–2002: relationship with soil moisture and effects of surface warming. *J Hydrometeorol* 5(6):1117–1130
- Dang H, Zhao Y, Chen X, Li J, Da G, Zhu Y (2004) Soil water characteristics in *Picea crassifolia* forestry lands in Qilian mountains. *Chin J Appl Ecol* 15(7):1148–1152
- Dean JS, Slaughter MC, Bowden DO (1996) Desert dendrochronology: tree-ring dating prehistoric sites in the Tucson Basin. *Kiva* 62(1):7–26
- Duffy JE, Mccarroll D, Barnes A, Ramsey CB, Davies D, Loader NJ, Miles D, Young GHF (2017) Short-lived juvenile effects observed in stable carbon and oxygen isotopes of UK oak trees and historic building timbers. *Chem Geol* 472:1–7
- Efron B (1979) Bootstrap methods: another look at the jackknife. *Ann Stat* 7:1–26
- Gong DY, Ho CH (2002) The Siberian high and climate change over middle to high latitude Asia. *Theor Appl Climatol* 72(1–2):1–9
- Guo Q, Cai J, Shao X, Sha W (2004) Studies on the variations of east-Asian summer monsoon during ad 1873–2000. *Chin J Atmos Sci* 28(2):206–215
- Guttman NB (1999) Accepting the standardized precipitation index: a calculation algorithm. *JAWRA J Am Water Resour Assoc* 35(2):311–322
- Harris I, Jones PD, Osborn TJ (2014) Updated high-resolution grids of monthly climatic observations—the CRU TS3.10 dataset. *Int J Climatol* 34(3):623–642
- Labuhn I, Daux V, Pierre M, Stievenard M, Girardclos O, Féron A (2014) Tree age, site and climate controls on tree ring cellulose $\delta^{18}\text{O}$: a case study on oak trees from south-western France. *Dendrochronologia* 32(1):78–89
- Leavitt SW (2010) Tree-ring C–H–O isotope variability and sampling. *Sci Total Environ* 408:5244
- Li Q, Nakatsuka T, Kawamura K, Liu Y, Song H (2011a) Regional hydroclimate and precipitation $\delta^{18}\text{O}$ revealed in tree-ring cellulose $\delta^{18}\text{O}$ from different tree species in semi-arid Northern China. *Chem Geol* 282:19–28
- Li Q, Nakatsuka T, Kawamura K, Liu Y, Song H (2011b) Hydroclimate variability in the North China Plain and its link with El Niño–Southern Oscillation since 1784 A.D.: insights from tree-ring cellulose $\delta^{18}\text{O}$. *J Geophys Res Atmos* 116:D22106. <https://doi.org/10.1029/2011JD015987>

- Li Q, Liu Y, Song H, Cai Q, Yang Y (2013) Long-term variation of temperature over north china and its links with large-scale atmospheric circulation. *Quat Int* 283(283):11–20
- Li J, Shi P, Zhu G, He Y, Liu Y, Tong H, Yang L (2015a) Characteristics of $\delta^{18}\text{O}$ in precipitation and moisture transports in the central Hexi Corridor. *Acta Sci Circumst* 35:947–955
- Li Q, Liu Y, Nakatsuka T, Song H, Mccarroll D, Yang Y, Qi J (2015b) The 225-year precipitation variability inferred from tree-ring records in shanxi province, the north china, and its teleconnection with Indian summer monsoon. *Glob Planet Change* 132:11–19
- Liu X, Shaffer L (2007) Connections across Eurasia: transportation, communication, and cultural exchange on the Silk Roads. *Explor World Hist* 3:119–120
- Liu Y, Cai Q, Liu W, Yang Y, Sun J, Song H, Li X (2008) Monsoon precipitation variation recorded by tree-ring $\delta^{18}\text{O}$ in arid Northwest China since AD 1878. *Chem Geol* 252:56–61
- Liu Y, Xie L, Li Q, Cai Q (2012a) Growth-climate response analysis between tree-ring width and March–September mean minimum temperature in Dongda Mountain, Gansu, China since 1820 AD. *J Earth Environ* 3:900–907
- Liu X, An W, Treydte K, Shao X, Leavitt S, Hou S, Chen T, Sun W, Qin D (2012b) Tree-ring $\delta^{18}\text{O}$ in southwestern China linked to variations in regional cloud cover and tropical sea surface temperature. *Chem Geol* 291:104–115
- Liu Y, Lei Y, Sun B, Song H, Sun J (2013a) Annual precipitation in Liancheng, China, since 1777 AD derived from tree rings of Chinese pine (*Pinus tabulaeformis* Carr.). *Int J Biometeorol* 57:927–934
- Liu Y, Sun B, Song H, Lei Y, Wang C (2013b) Tree-ring-based precipitation reconstruction for Mt. Xinglong, China, since AD 1679. *Quat Int* 283:46–54
- Liu Y, Sun C, Li Q, Cai Q (2016) A *Picea crassifolia* tree-ring width-based temperature reconstruction for the Mt. Dongda Region, Northwest China, and its relationship to large-scale climate forcing. *PLoS One* 11(8):e0160963. <https://doi.org/10.1371/journal.pone.0160963>
- Loader NJ, Robertson I, Barker AC, Switsur VR, Waterhouse JS (1997) An improved technique for the batch processing of small whole-wood samples to α -cellulose. *Chem Geol* 136:313–317
- Ma N, Wang N, Zhu J, Chen X, Chen H, Dong C (2011) Climate change around the Badain Jaran Desert in recent 50 years. *J Desert Res* 31(6):1541–1547
- McCarroll D, Loader NJ (2004) Stable isotopes in tree rings. *Quat Sci Rev* 23:771–801
- Miehe G, Miehe S, Martin W, Lars O, La D, Tsering D et al (2008) An inventory of forest relicts in the pastures of southern Tibet (Xizang A.R. China). *Plant Ecol* 194(2):157–177
- Nakatsuka T, Ohnishi K, Hara T, Sumida A, Mitsuishi D, Kurita N, Uemura S (2008) Oxygen and carbon isotopic ratios of tree-ring cellulose in a conifer-hardwood mixed forest in northern Japan. *Geochem J* 38:77–88
- Olson E, Dodd J, Rivera M (2017) Climate variability over the Holocene in the Atacama Desert of Chile as reconstructed from tree ring isotope series. In: EGU general assembly conference abstracts, 2017
- Qin C, Bao Y, Bräuning A, Griesinger J, Wernicke J (2015) Drought signals in tree-ring stable oxygen isotope series of Qilian juniper from the arid northeastern Tibetan Plateau. *Glob Planet Change* 125:48–59
- Quenouille MH (1949) Problems in plane sampling. *Ann Math Stat* 20(3):355–375
- Ramesh R, Bhattacharya SK, Gopalan K (1985) Dendroclimatological implications of isotope coherence in trees from Kashmir Valley, India. *Nature* 317:802–804
- Roden JS, Lin G, Ehleringer JR (2000) A mechanistic model for interpretation of hydrogen and oxygen isotope ratios in tree-ring cellulose. *Geochim Cosmochim Acta* 64:21–35
- Sano M, Sheshshayee MS, Managave S, Ramesh R, Sukumar R, Sweda T (2010) Climatic potential of $\delta^{18}\text{O}$ of *Abies spectabilis* from the Nepal Himalaya. *Dendrochronologia* 28:93–98
- Shi C, Daux V, Zhang Q-B, Risi C, Hou S-G, Stievenard M, Pierre M, Li Z, Delmotte M, V (2012) Reconstruction of southeast Tibetan Plateau summer climate using tree ring $\delta^{18}\text{O}$: moisture variability over the past two centuries. *Clim Past* 8:205–213
- Su Q, Lu R (2014) Teleconnection between rainfall over South China and the East European Plain in July and August. *Theor Appl Climatol* 118(1–2):185–194
- Tan L, Cai Y, An Z, Zhang H (2011) Climate patterns in north central China during the last 1800 year and its possible driving force. *Clim Past Discuss* 7:685–692
- Treydte KS, Schleser GH, Helle G, Frank DC, Winiger M, Haug GH, Esper J (2006) The twentieth century was the wettest period in northern Pakistan over the past millennium. *Nature* 440:1179–1182
- Tsuji H, Nakatsuka T, Takagi K (2006) $\delta^{18}\text{O}$ of tree-ring cellulose in two species (spruce and oak) as proxies of precipitation amount and relative humidity in northern Japan. *Chem Geol* 231(1–2):67–76
- Vuille M, Werner M, Bradley RS, Keimig F (2005) Stable isotopes in precipitation in the Asian monsoon region. *J Geophys Res Atmos* 110:3345–3356
- Wang WZ, Liu XH, Xu GB, Shao XM, Qin DH, Sun WZ, An WL, Zeng XM (2013) Moisture variations over the past millennium characterized by Qaidam Basin tree-ring $\delta^{18}\text{O}$. *Chin Sci Bull* 58:3956–3961
- Wernicke J, Hochreuther P, Griesinger J, Zhu H, Wang L, Bräuning A (2017a) Multi-century humidity reconstructions from the southeastern Tibetan Plateau inferred from tree-ring $\delta^{18}\text{O}$. *Glob Planet Change* 149:26–35
- Wernicke J, Hochreuther P, Griesinger J, Zhu H, Wang L, Bräuning A (2017b) Air mass origin signals in $\delta^{18}\text{O}$ of tree-ring cellulose revealed by back-trajectory modeling at the monsoonal Tibetan plateau. *Int J Biometeorol* 61(6):1–16
- White JWC, Cook ER, Lawrence JR, Wallaces B (1985) The D/H ratio of sap in trees: Implications for water resources and tree D/H ratios. *Geochim Cosmochim Acta* 49:237–246
- Wigley TML, Briffa KR, Jones PD (1984) On the average value of correlated time series, with applications in dendroclimatology and hydrometeorology. *J Climatol Appl Meteorol* 23:201–213
- Willett KM, Jones PD, Gillett NP (2008) Recent changes in surface humidity: development of the HadCRUH dataset. *J Clim* 21(20):5364–5383
- Xu G, Chen T, Liu X, An W, Wang W, Yun H (2011) Potential linkages between the moisture variability in the northeastern Qaidam Basin, China, since 1800 and the East Asian summer monsoon as reflected by tree ring $\delta^{18}\text{O}$. *J Geophys Res Atmos*. <https://doi.org/10.1029/2010JD015053>
- Xu C, Pumijumong N, Nakatsuka T, Sano M, Li Z (2015a) A tree-ring cellulose $\delta^{18}\text{O}$ -based July–October precipitation reconstruction since AD 1828, northwest Thailand. *J Hydrol* 529:433–441
- Xu G, Liu X, Wu G, Chen T, Wang W, Zhang Q, Zhang Y, Zeng X, Qin D, Sun W (2015b) Tree ring $\delta^{18}\text{O}$'s indication of a shift to a wetter climate since the 1880s in the western Tianshan Mountains of northwestern China. *J Geophys Res Atmos* 120:6409–6425
- Xu G, Liu X, Trouet V, Treydte K, Wu G, Chen T (2018) Regional drought shifts (1710–2010) in East Central Asia and linkages with atmospheric circulation recorded in tree-ring $\delta^{18}\text{O}$. *Clim Dyn*. <https://doi.org/10.1007/s00382-018-4215-2>
- Yang XP, Ma N, Dong JF, Zhu BQ, Xu B, Ma ZB, Liu JQ, Yang XP, Scuderi LA (2010) Recharge to the inter-dune lakes and Holocene

- climatic changes in the Badain Jaran Desert, Western China. *Quat Res* 73:10–19
- Yang B, Qin C, Bräuning A, Burchardt I, Liu J (2011) Rainfall history for the Hexi corridor in the arid northwest china during the past 620 years derived from tree rings. *Int J Climatol* 31(8):1166–1176
- Yi L, Yu H, Ge J, Lai Z, Xu X, Qin L, Peng S (2012) Reconstructions of annual summer precipitation and temperature in north-central China since 1470 AD based on drought/flood index and tree-ring records. *Clim Change* 110:469–498
- Young GHF, Demmler JC, Gunnarson BE, Kirchhefer AJ, Loader NJ, McCarroll D (2011) Age trends in tree ring growth and isotopic archives: a case study of *Pinus sylvestris* L. from northwestern Norway. *Glob Biogeochem Cycles*. <https://doi.org/10.1029/2010GB003913>
- Yu Y, Yang T, Li J, Liu J, An C, Liu X et al (2006) Millennial-scale holocene climate variability in the nw china drylands and links to the tropical pacific and the north atlantic. *Palaeogeogr Palaeoclimatol Palaeoecol* 233(1):149–162